

Research

Open Access

A multiscale mathematical model of cancer, and its use in analyzing irradiation therapies

Benjamin Ribba*¹, Thierry Colin² and Santiago Schnell³

Address: ¹Institute for Theoretical Medicine and Clinical Pharmacology Department, Faculty of Medicine R.T.H Laennec, University of Lyon, Paradin St., P.O.B 8071, 69376 Lyon Cedex 08, France, ²Mathématiques Appliquées de Bordeaux, CNRS UMR 5466 and INRIA futurs, University of Bordeaux 1, 351 cours de la liberation, 33405 Talence Cedex, France and ³Indiana University School of Informatics and Biocomplexity Institute, 1900 East Tenth Street, Eigenmann Hall 906, Bloomington, IN 47406, USA

Email: Benjamin Ribba* - ribba@upcl.univ-lyon1.fr; Thierry Colin - colin@math.u-bordeaux.fr; Santiago Schnell - schnell@indiana.edu

* Corresponding author

Published: 10 February 2006

Received: 28 September 2005

Theoretical Biology and Medical Modelling 2006, **3**:7 doi:10.1186/1742-4682-3-7

Accepted: 10 February 2006

This article is available from: <http://www.tbiomed.com/content/3/1/7>

© 2006 Ribba et al; licensee BioMed Central Ltd.

This is an Open Access article distributed under the terms of the Creative Commons Attribution License (<http://creativecommons.org/licenses/by/2.0>), which permits unrestricted use, distribution, and reproduction in any medium, provided the original work is properly cited.

Abstract

Background: Radiotherapy outcomes are usually predicted using the Linear Quadratic model. However, this model does not integrate complex features of tumor growth, in particular cell cycle regulation.

Methods: In this paper, we propose a multiscale model of cancer growth based on the genetic and molecular features of the evolution of colorectal cancer. The model includes key genes, cellular kinetics, tissue dynamics, macroscopic tumor evolution and radiosensitivity dependence on the cell cycle phase. We investigate the role of gene-dependent cell cycle regulation in the response of tumors to therapeutic irradiation protocols.

Results: Simulation results emphasize the importance of tumor tissue features and the need to consider regulating factors such as hypoxia, as well as tumor geometry and tissue dynamics, in predicting and improving radiotherapeutic efficacy.

Conclusion: This model provides insight into the coupling of complex biological processes, which leads to a better understanding of oncogenesis. This will hopefully lead to improved irradiation therapy.

Background

Mathematical models of cancer growth have been the subject of research activity for many years. The Gompertzian model [1,2], logistic and power functions have been extensively used to describe tumor growth dynamics (see for example [3] and [4]). These simple formalisms have been also used to investigate different therapeutic strategies such as antiangiogenic or radiation treatments [5].

The so-called linear-quadratic (LQ) model [6] is still extensively used, particularly in radiotherapy, to study

damage to cells by ionizing radiation. Indeed, extensions of the LQ model such as the 'Tumor Control Probability' model [7] are aimed at predicting the clinical efficacy of radiotherapeutic protocols. Typically, these models assume that tumor sensitivity and repopulation are constant during radiotherapy. However, experimental evidence suggests that cell cycle regulation is perhaps the most important determinant of sensitivity to ionizing radiation [8]. It has been suggested that anti-growth signals such as hypoxia or the contact effect, which are

Structural Integration axis

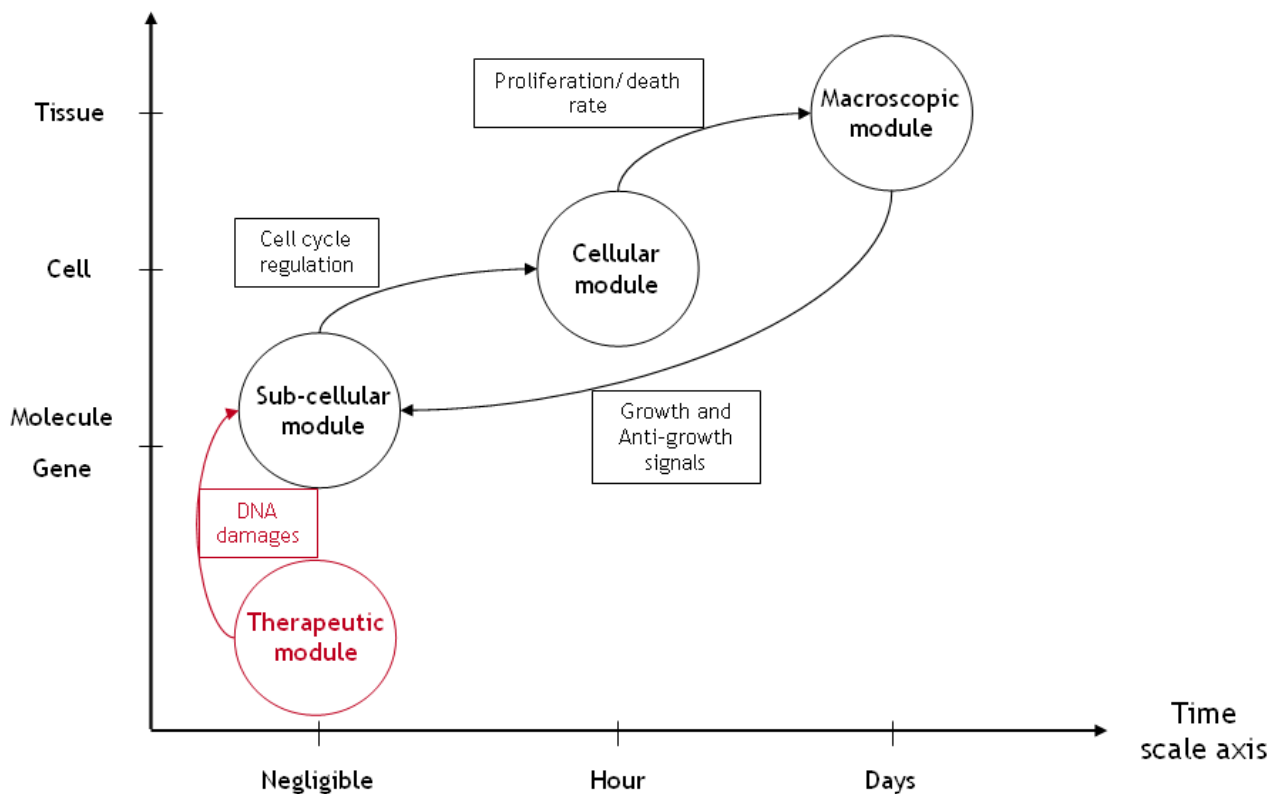


Figure 1
Multiscale nature of the model. Schematic view of the multiscale nature of the model, composed of four different levels. At the genetic level we integrate the main genes involved in the evolution of colorectal cancer within a Boolean network and this results in cell cycle regulation signals. The response to these signals occurs at the cellular level, determining whether each cell proliferates or dies. Given this information, the macroscopic model the new spatial distribution of the cells is computed at the tissue level. The number and spatial configuration of cells determine the activation of the antigrowth signals, which in turn is input to the genetic level. Irradiation induces DNA breaks, which, in the model, activate the $p53$ gene at the genetic level.

responsible for decreasing the growth fraction, may play a crucial role in the response of tumors to irradiation [9].

Nowadays, computational power allows us to build mathematical models that can integrate different aspects of the disease and can be used to investigate the role of complex tumor growth features in the response to therapeutic protocols [10]. In the present study we propose a multiscale model of tumor evolution to investigate growth regulation in response to radiotherapy. In our model, key genes in colorectal cancer have been integrated within a Boolean genetic network. Outputs of this genetic model have been linked to a discrete model of the cell cycle where cell radiosensitivity has been assumed to be cycle phase specific. Finally, Darcy's law has been used to simulate macroscopic tumor growth.

The multiscale model takes into account two key regulation signals influencing tumor growth. One is hypoxia, which appears when cells lack oxygen. The other is overpopulation, which is activated when cells do not have sufficient space to proliferate. These signals have been correlated to specific pathways of the genetic model and integrated up to the macroscopic scale.

Methods

Oncogenesis is a set of sequential steps in which an interplay of genetic, biochemical and cellular mechanisms (including gene pathways, intracellular signaling pathways, cell cycle regulation and cell-cell interactions) and environmental factors cause normal cells in a tissue to develop into a tumor. The development of strategies for treating oncogenesis relies on the understanding of patho-

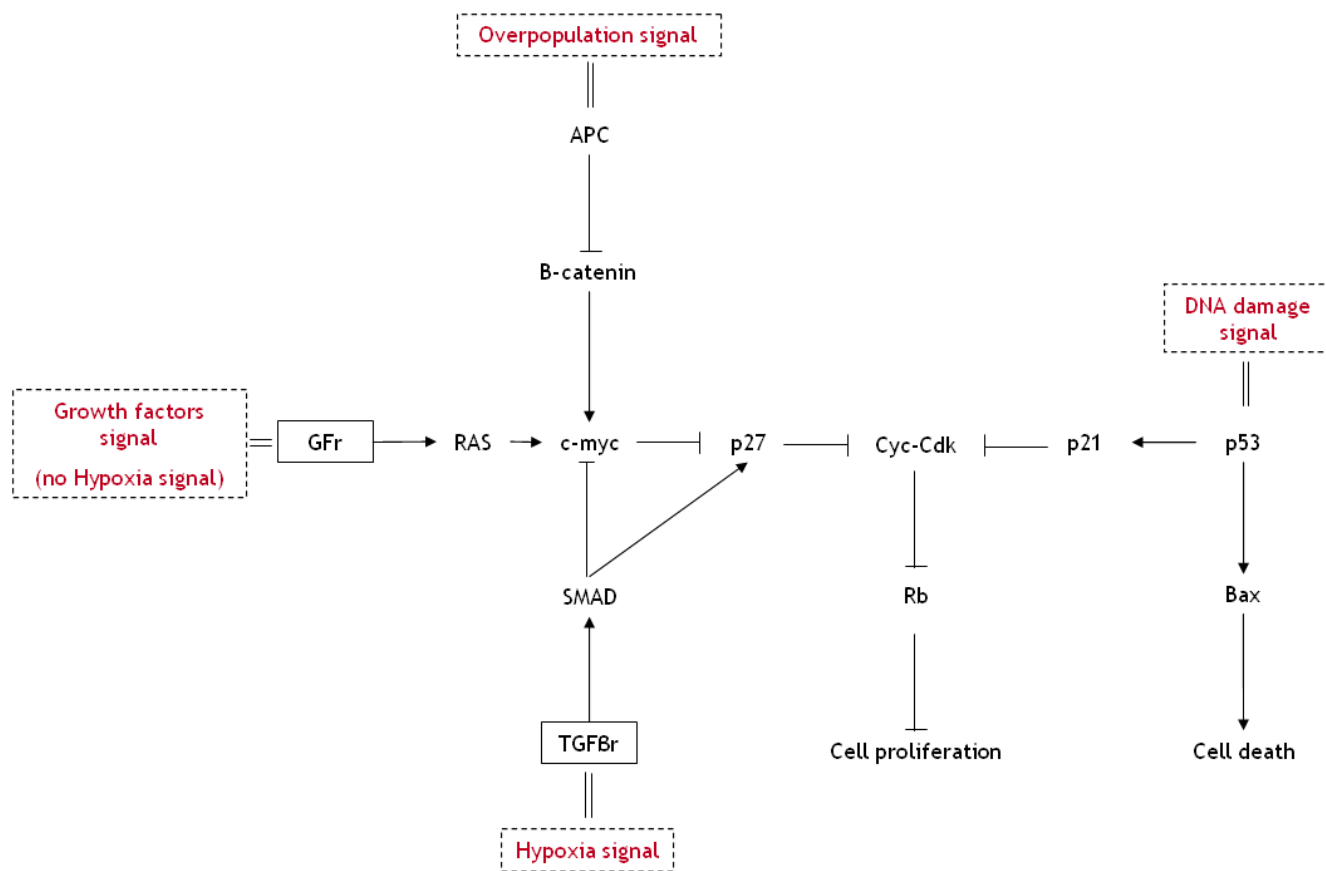


Figure 2
Cell proliferation and death (genetic regulation) for colorectal cancer. This figure shows the genetic model with regulation signals as inputs. *p53* is activated when DNA is damaged and leads the cell to apoptosis. *SMAD* is activated through *TGFβ* receptors during hypoxia and inhibits cell proliferation. Overpopulation inhibits cell proliferation through activation of *APC*. *RAS* promotes cell proliferation through growth factor receptors when sufficient oxygen is available for the cell, that is, there is no hypoxia. This flow chart was developed from knowledge available from bibliographic resources [15,16] and from the Knowledge Encyclopedia of Genes and Genomes [53,54].

genesis at the cellular and molecular levels. We have therefore developed a multiscale mathematical model of these processes to study the efficacy of radiotherapy. Several mathematical frameworks have been developed to model avascular and vascular tumor growth (see [11-14]). Here we propose a multiscale mathematical model for avascular tumor growth, which is schematically presented in Figure 1. This model provides a powerful tool for addressing questions of how cells interact with each other and their environment. We use the model to study tumor regression during radiotherapy.

Gene level

Five genes are commonly mutated in colorectal cancer patients, namely: *APC* (Adenomatosis Polyposis Coli), *K-RAS* (Kirsten Rat Sarcoma viral), *TGF* (Transforming

Growth Factor), *SMAD* (Mothers Against Decapentaplegic) and *p53* or *TP53* (Tumor Protein 53). These genes belong to four specific pathways, which funnel external or internal signals that cause cell proliferation or cell death (see [15] and [16,17] for more details).

The anti-growth, *p53*, pathway is activated in the case of DNA damage [18,19]. This is particularly relevant during irradiation [20]. *p53* pathway activation can block the cell cycle and induce apoptosis [21,22]. The *K-RAS* gene belongs to a mitogenic pathway that promotes cell proliferation in the presence of growth factors [23]. Activation of the anti-growth pathways *TGFβ/SMAD* and *WNT/APC* inhibits cell proliferation. The *SMAD* gene is activated by hypoxia signals [24,25], while *APC* is activated through *β*-catenin by loss of cell-cell contact [26-30]. Moreover, it

Table 1: Apoptotic activity. Apoptotic activity induced by two 20 Gy radiotherapy protocols applied to APC-mutated tumor cells.

Apoptotic activity				
	Total dose (Gy)	Scheduling	Apoptotic fraction – mean – (%)	Apoptotic fraction – max – (%)
Standard protocol	20	2 Gy daily	2.59	4
Heuristic	20	2 Gy Repeated 10 times before hypoxia	3.14	4.25

has recently been hypothesized that overpopulation of APC mutated cells can explain the shifts of normal proliferation in early colon tumorigenesis [31].

We assume that activation of APC and SMAD is due to overpopulation and hypoxia signals respectively. Both pathways inhibit cell proliferation. In consequence, APC mutated cells promote overpopulation and SMAD or RAS mutated cells promote proliferation during hypoxia. Figure 2 shows the schematic genetic model.

We develop a Boolean model of these pathways in Figure 2. Each gene is represented by a node in the network and

Table 2: Genetic model. Boolean (logical) functions used in the genetic model depicted Figure 1. For APC, SMAD and RAS, Boolean values are set to 0, 0 and 1 respectively when genes are mutated.

Boolean model	
Node	Boolean updating function
APC ^t	$APC^{t+1} = \begin{cases} 1 & \text{if Overpopulation signal} \\ 0 & \text{otherwise} \end{cases}$
	APC ^{t+1} = 0 if mutated
βcat ^t	βcat ^{t+1} = ¬APC ^t
cmyc ^t	cmyc ^{t+1} = RAS ^t ∧ βcat ^t ∧ ¬SMAD ^t
p27 ^t	p27 ^{t+1} = SMAD ^t ∨ ¬cmyc ^t
p21 ^t	p21 ^{t+1} = p53 ^t
Bax ^t	Bax ^{t+1} = p53 ^t
SMAD ^t	$SMAD^{t+1} = \begin{cases} 1 & \text{if Hypoxia signal} \\ 0 & \text{otherwise} \end{cases}$
	SMAD ^{t+1} = 0 if mutated
RAS ^t	$RAS^{t+1} = \begin{cases} 1 & \text{if no Hypoxia signal} \\ 0 & \text{otherwise} \end{cases}$
	RAS ^{t+1} = 1 if mutated
p53 ^t	$p53^{t+1} = \begin{cases} 1 & \text{if DNA damage signal} \\ 0 & \text{otherwise} \end{cases}$
	p53 ^{t+1} = 0 if mutated
CycCDK ^t	CycCDK ^{t+1} = ¬p21 ^t ∧ ¬p27 ^t
Rb ^t	Rb ^{t+1} = ¬CycCDK ^t

the interactions are encoded as the edges. The state of each node is 1 or 0, corresponding to the presence or absence of the genetic species. The state of a node can change with time according to a logical function of its state and the states of other nodes with edges incident on it [32-34]. The rules governing the genetic pathways are presented in Table 2.

Cell level

We consider a discrete mathematical model of the cell cycle in which the cycle phase duration values were set according to the literature [35]. In our model the proliferative cycle is composed of three distinct phases: S (DNA synthesis), G₁ (Gap 1) and G₂M (Mitosis). We model the 'Restriction point' R [36] at the end of G₁ where internal and external signals, i.e. cell DNA damage, overpopulation and hypoxia, are checked [37] (see Figure 3 for a schematic representation of our cell cycle model).

For each spatial position (x, y), we assume that:

- If the local concentration of oxygen is below a constant threshold Th_o and if SMAD is not mutated, hypoxia is declared and causes cells to quiesce (G₀) through SMAD gene activation (see Figure 2);
- If the local number of cells is above a constant threshold Th₁ and if APC is not mutated, overpopulation is declared and leads cells to quiesce (G₀) through the APC gene (see Figure 2);
- Otherwise, if the conditions are appropriate, cells enter G₂M and divide, generating new cells at the same spatial position.

Induction of apoptosis through p53 gene activation is discussed later.

Tissue level

We use a fluid dynamics model to describe tissue behavior. This macroscopic-level continuous model is based on Darcy's law, which is a good model of the flow of tumor cells in the extracellular matrix [38-40]:

$$v = -k\nabla p \quad (1)$$

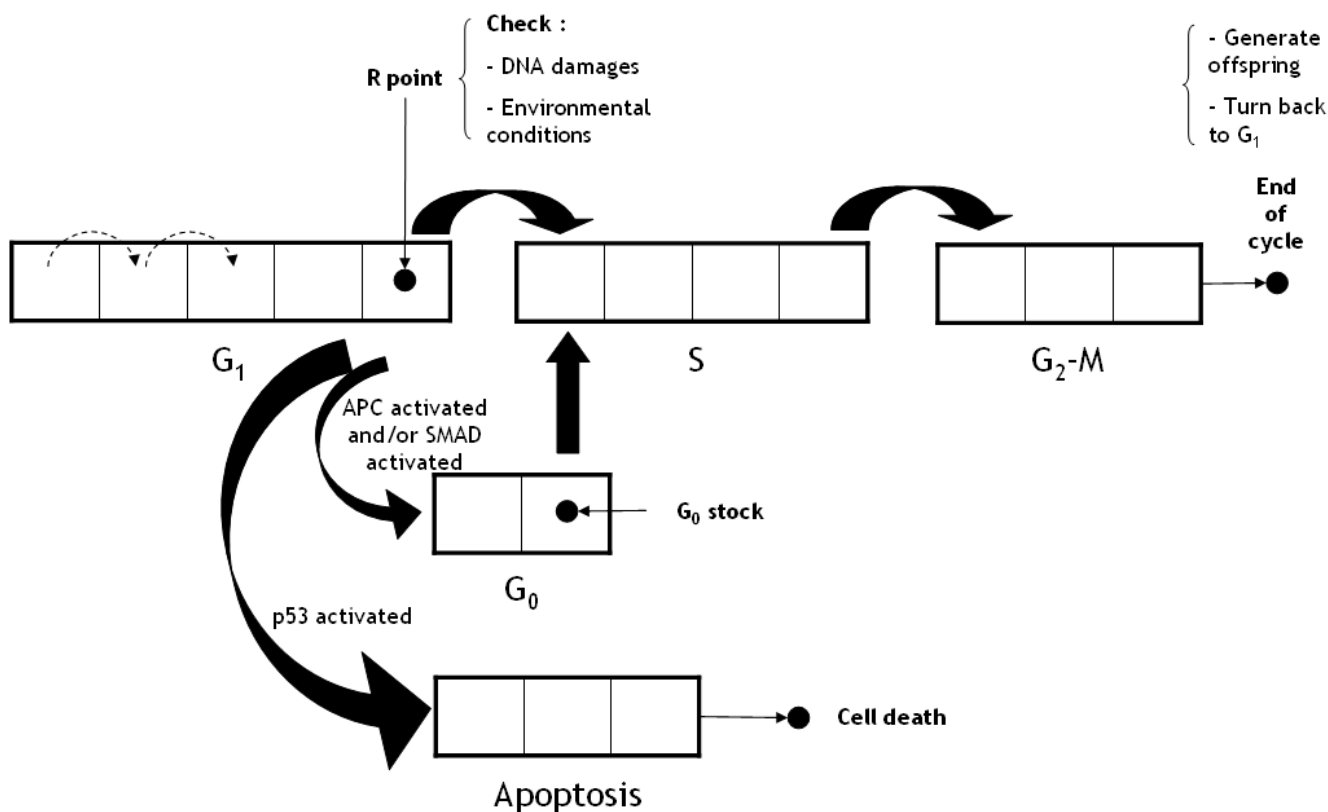


Figure 3

Diagram of the cell cycle model. In this discrete model, cells progress through a cell cycle comprising three phases: G_1 , S , and G_2M . At the end of the G_2M phase, cells divide and new cells begin their cycle in G_1 . At the last stage of phase G_1 , we modelled the restriction point R , where DNA integrity and external conditions (overpopulation and hypoxia) are checked. If overpopulation occurs, APC is activated; if hypoxia occurs, $SMAD$ is activated. Both these conditions lead cells to G_0 (quiescence). Cells remain in the quiescent phase in the absence of external changes, otherwise they may return to the proliferative cycle (at the first step of S phase). DNA damage can also activate the $p53$ pathway, which leads cells to the apoptotic phase. Cells at the end of the apoptotic phase die and disappear from the computational domain.

where p is the pressure field. The media permeability k is assumed to be constant.

We study the evolution of the cell densities in two dimensions. We formulate the cell densities in the tissue mathematically as advection equations, where $n_\phi(x, y, t)$ represents the density of cells with position (x, y) at time t in a given cycle phase ϕ . Assuming that all cells move with the same velocity given by Eq. (1) and applying the principle of mass balance, the advection equations are:

$$\frac{\partial n_\phi}{\partial t} + \nabla \cdot (vn_\phi) = P_\phi \quad \forall \phi \in \{G_1, S, G_2M, G_0, Apop\} \quad (2)$$

where P_ϕ is the cell density proliferation term in phase ϕ at time t , retrieved from the cell cycle model.

The global model is an age-structured model (see Section 2.7). Initial conditions for n_ϕ are presented in Section 2.6.

Assuming $\sum_\phi n_\phi$ to be a constant and adding Eq. (2) for all phases, the pressure field p satisfies:

$$-\nabla \cdot (k\nabla p) = \sum_\phi P_\phi. \quad (3)$$

The pressure is constant on the boundary of the computational domain.

In our model, the oxygen concentration C follows a diffusion equation with Dirichlet conditions on the edge of the computation domain Ω .

$$\frac{\partial C}{\partial t} - \nabla \cdot (D\nabla C) = -\sum_\phi \alpha_\phi n_\phi \quad \text{on } \Omega/\Omega_{bv} \quad (4)$$

$$C = C_{\max} \quad \text{on } \Omega_{bv} \quad (5)$$

Table 3: Table of parameters Table of numerical parameters used for simulations.

Model parameters				
Parameter	Description	Unit	Value	Reference
T_{G_1}	Duration of G_1 phase	h	20	[35,44]
T_S	Duration of S phase	h	10	[35,44]
T_{G_2M}	Duration of G_2M phase	h	3	[35,44]
T_{G_0}	Duration of G_0 phase	h	5	Estimated
$T_{Apoptosis}$	Duration of the apoptotic phase	h	5	Estimated
C_{max}	Oxygen in blood	mlO_2	10^{-2}	Estimated
α_ϕ	Oxygen consumption in phase ϕ	mlO_2s^{-1}	$5 - 10 \times 10^{-15}$	Estimated
Th_o	Hypoxia threshold	$cell^{-1}$	5×10^{-15}	Estimated
Th_t	Overpopulation threshold	$cell$	2000	Estimated
R_ϕ	Cell Radio-sensitivity in phase ϕ	Gy^{-1}	0.2 – 2	[41-43]
k	Media permeability	m^2	0.2	Estimated

$$C_{\partial\Omega} = 0 \quad (6)$$

D is the oxygen diffusion coefficient, which is constant throughout the computation domain. In this equation, Ω_{bv} stands for the spatial location of blood vessels, α_ϕ is the coefficient of oxygen uptake by cells at cell cycle phase ϕ and C_{max} is the constant oxygen concentration in blood vessels.

Therapy assumptions

Cell sensitivity depends on cell cycle phase [8]. We assume that only proliferative cells are sensitive to the treatment. In addition, we assume that DNA damage is proportional to the irradiation dose. This is known as the 'single hit' theory, which is governed by the expression

$$n_{dsb} = R_\phi d \quad (7)$$

where n_{dsb} is the number of double strand breaks induced by radiation dose d . As mentioned previously, the radiosensitivity R_ϕ has been assumed to depend on the cell cycle phase (see Table 3). Based upon radiobiological experiments found in the literature, we take the radiosensitivity as constant ($2 Gy^{-1}$) in G_1 and G_0 . It decreases in S phase to $0.2 Gy^{-1}$, and then increases to $2 Gy^{-1}$ during G_2 .

We set a constant treatment threshold Th_r , such that if n_{dsb} due to the irradiation dose is above Th_r at any time, $p53$ is activated and the cells are labeled as 'DNA damaged cells'. DNA damaged cells are identified at the R point of the cell cycle and are directed to apoptosis. They die and disappear from the computational domain after $T_{Apoptosis}$, i.e. the duration of the apoptotic phase.

The standard radiotherapy protocol used in the simulations consists of a 2 Gy dose delivered each day, five days a week, and can be repeated for several weeks. The radiotherapeutic dose is assumed to be uniformly distributed over the spatial domain.

According to the radiosensitivity parameters found in the literature [41-43], only a fraction of mitotic cells are assumed to be sensitive to the standard 2 Gy dose.

Model parameters

Cell cycle kinetic parameters were retrieved from flow cytometric analysis of human colon cancer cells [35,44]. Table 3 summarizes the quantitative parameters used in our model.

Computational domain and initial conditions

In our two-dimensional model we study an 8 cm square tissue. We assume that the domain comprises five small circular tumor masses, the first located at the center of the computational domain and the other four towards the corners. Moreover, the domain has two sources of oxygen, to the right and left sides of the central cell cluster (see Figure 4).

The number of cells in each tumor is the same, and they are uniformly distributed. The number of cells in each phase of the cell cycle is proportional to the duration of the phase. For instance, the G_1 phase contains twice as many cells as the S phase because the G_1 phase is twice as long as the S phase. It is important to emphasize that the cell cycle phases are discrete (see Section 2.7).

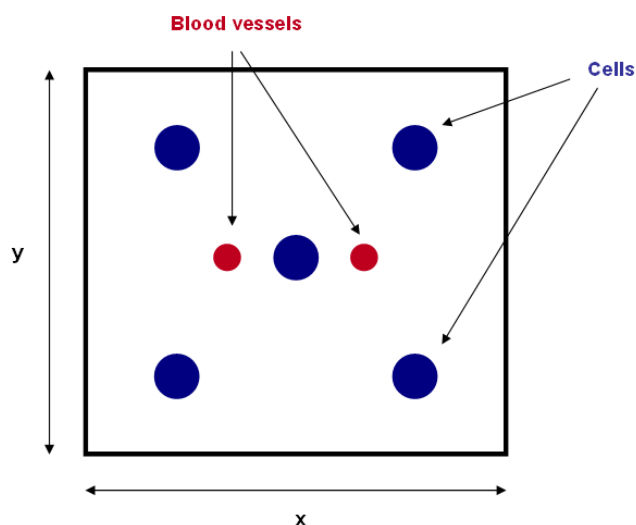


Figure 4
Initial conditions. Schematic representation of the two-dimensional computation domain for model simulations, with the initial spatial configuration of the cells. The domain is composed of five cell clusters and two blood vessels.

Simulation technique

The model is fully deterministic. Cell cycle phases durations τ_ϕ have been discretized in several elementary age intervals $a \in \{1, \dots, N_\phi\}$ where N_ϕ is an integer such as $\tau_\phi = dt \times N_\phi$. Here dt is the time step of the cell cycle model. The cell density $n_{a,\phi}$ at age a in phase ϕ is governed by:

$$\frac{\partial n_{a,\phi}}{\partial t} + \nabla \cdot (vn_{a,\phi}) = P_{a,\phi}. \tag{8}$$

In this equation, $\phi \in \{G_1, S, G_2M, G_0, Apoptosis\}$ and $a \in \{1, \dots, N_\phi\}$. $P_{a,\phi}$ is the cell density proliferation term in phase ϕ at age a retrieved from the cell cycle model. In the simulations, the intracellular and extracellular conditions were identified for cells at the end of G_1 phase. These were used as initial conditions for the gene level model. The genetic model was computed until it reached steady state (this is of the order of 10 iterations).

Noting that $\sum_{a,\phi} n_{a,\phi}$ is constant, we can sum Eqs. (8) to obtain an expression for the pressure field of the form:

$$-\nabla \cdot (k\nabla p) = \sum_{a,\phi} P_{a,\phi}. \tag{9}$$

The computer program starts from an initial distribution of cells in each state $\{a, \phi\}$. The computations are performed using a splitting technique. First we run the cell cycle model for one time-step dt , then retrieve new values for $n_{a,\phi}$ and compute $P_{a,\phi}$. Pressure is retrieved by solving

Eq. (9) and velocity is computed using Darcy's law (see Eq. (1)). Since the contribution of the source term has been taken into account by the cell cycle model at the first stage of the splitting technique, Eqs. (8) are solved continuously and without second members:

$$\frac{\partial n_{a,\phi}}{\partial t} + \nabla \cdot (vn_{a,\phi}) = 0, \tag{10}$$

which can also be written [using (9)]:

$$\frac{\partial n_{a,\phi}}{\partial t} + v \cdot \nabla n_{a,\phi} = \left(\sum_{a',\phi'} P_{a',\phi'} \right) n_{a,\phi}. \tag{11}$$

This equation is then solved using a splitting technique. The advection parts of Eq. (11) are solved by sub-cycling finite different scheme computations, with time-step dt_{adv} being smaller than dt (for stability reasons). We set $n_{a,\phi} = 0$ on the part of the boundary where $v \cdot \nu < 0$, ν denoting the outgoing normal to the boundary. For the pressure p , we set $p = 0$ on the boundary.

All simulations (except the ones shown in Figure 7) were run for 320 h with time step $dt = 1 h$ in a discrete computational domain composed by 100×100 elementary spatial units.

Results and discussion

We divide our results and discussion into three parts. The first section concerns simulations of the model without therapeutic interactions (Sections 3.1–3.2). The second part deals with the interactions between tumor growth and the effect of therapeutic protocols (Section 3.3). Finally, we investigate the sensitivity of the results to model parameters and initial conditions (Section 3.4). Genetic mutations are simulated by running the model, having set the Boolean values of particular genes constant (see Table 2). Since the genetic model is run until steady state is reached, simulation of mutated cell growth is equivalent to simulation of cells that are not sensitive to particular anti-growth signals. In the following, we will refer to cells with at least one mutation as 'cancer cells'. Cells with no mutations are called 'normal cells'.

Gene-dependent tumor growth regulation

Figure 5 shows the simulated growth of cell colonies. According to the model settings, the colony of normal cells grows up to 10^6 cells and is then regulated through activation of gene *APC* owing to overpopulation. *APC* mutated tumor cells are not sensitive to overpopulation and reproduce exponentially until late regulation because of hypoxia, through *SMAD* gene activation. Finally, according to the model parameters, *APC* and *SMAD/RAS*

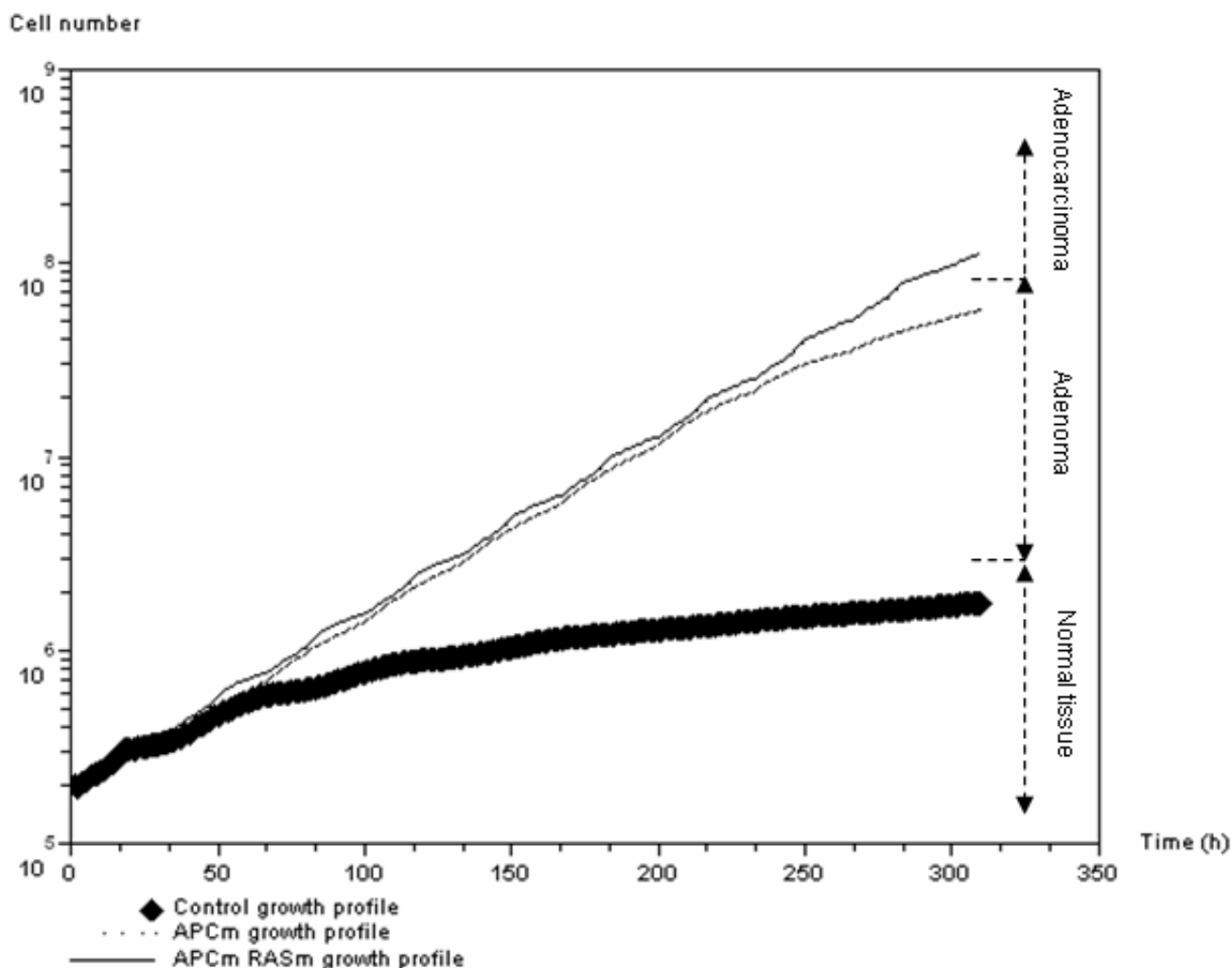


Figure 5
Cell population growth. Cell population growth (log plot) over time according to three different genetic profiles: normal cells (black diamonds), APC mutated cells (dashed line), and APC + SMAD/RAS mutated cells.

mutated tumor cells cannot be regulated at all and thus induce an exponential growth profile.

The simulation results reproduce the evolution of colorectal cancer [16,45]. Indeed, APC has been shown to promote shifts in pattern of the normal cell population in early colorectal tumorigenesis, and SMAD/RAS mutations promote evolution from early adenoma to adenocarcinoma.

Features of anti-growth signals and effect on tumor growth
 APC-dependent growth regulation

The top diagram of Figure 6 shows the evolution of the total and quiescent cell numbers, when population growth is regulated through activation of the APC gene

due to overpopulation. Figure 6 shows that the first 100 hours are characterized by oscillations in both populations, which slowly disappear and become linear growth. Indeed, as the cell population begins to grow, it tends to activate APC signaling owing to overpopulation in the inner part of the tumor masses. This results in a rapid increase in the number of quiescent cells, which in turn slows cell proliferation. Cell advection leads to invasion of new tissues, which promotes proliferation and in turn slows the evolution of the quiescent cell population. These oscillations in cell population are caused by a combination of overpopulation signal propagation in the inner parts of the cell clusters and the cells' ability to move to colonize free space. Very soon, what was once free space becomes overpopulated. This results in a constant propor-

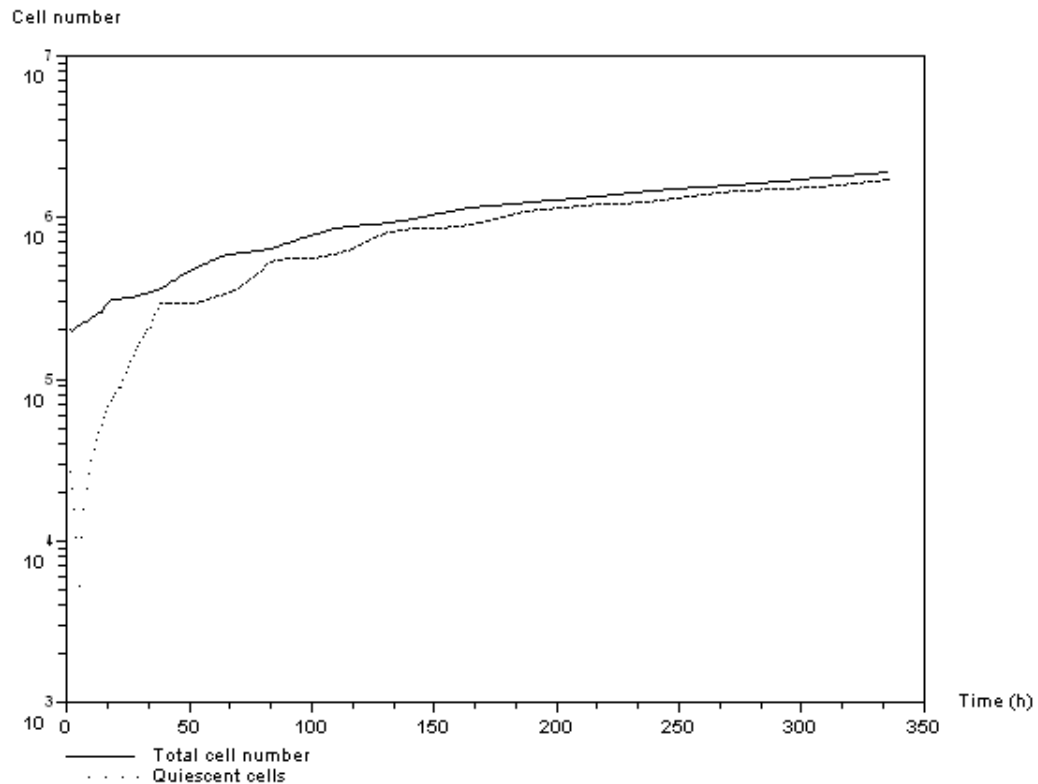


Figure 6

APC-dependent growth regulation. Top: Evolution of the number of quiescent cells and total number of cells over time (log plot). Cell population is regulated through APC activation owing to overpopulation. Total cell number (continuous line) and number of quiescent cells (dotted line). Bottom: Snapshots of cells within the computational domain during simulation ($t = 100$ h). Left: Total cell number. Right: Mitotic cells are only in the outer region of the tumor masses. Cells at the core are quiescent through APC activation due to overpopulation.

tion of new cells becoming quiescent (see the late phase of the curves Figure 6). The two snapshots presented at the bottom of Figure 6 show the spatial distribution of all

cells (left), and that of mitotic cells only (right). Mitotic cells are situated on the outer region owing to overpopulation in the central parts of the clusters.

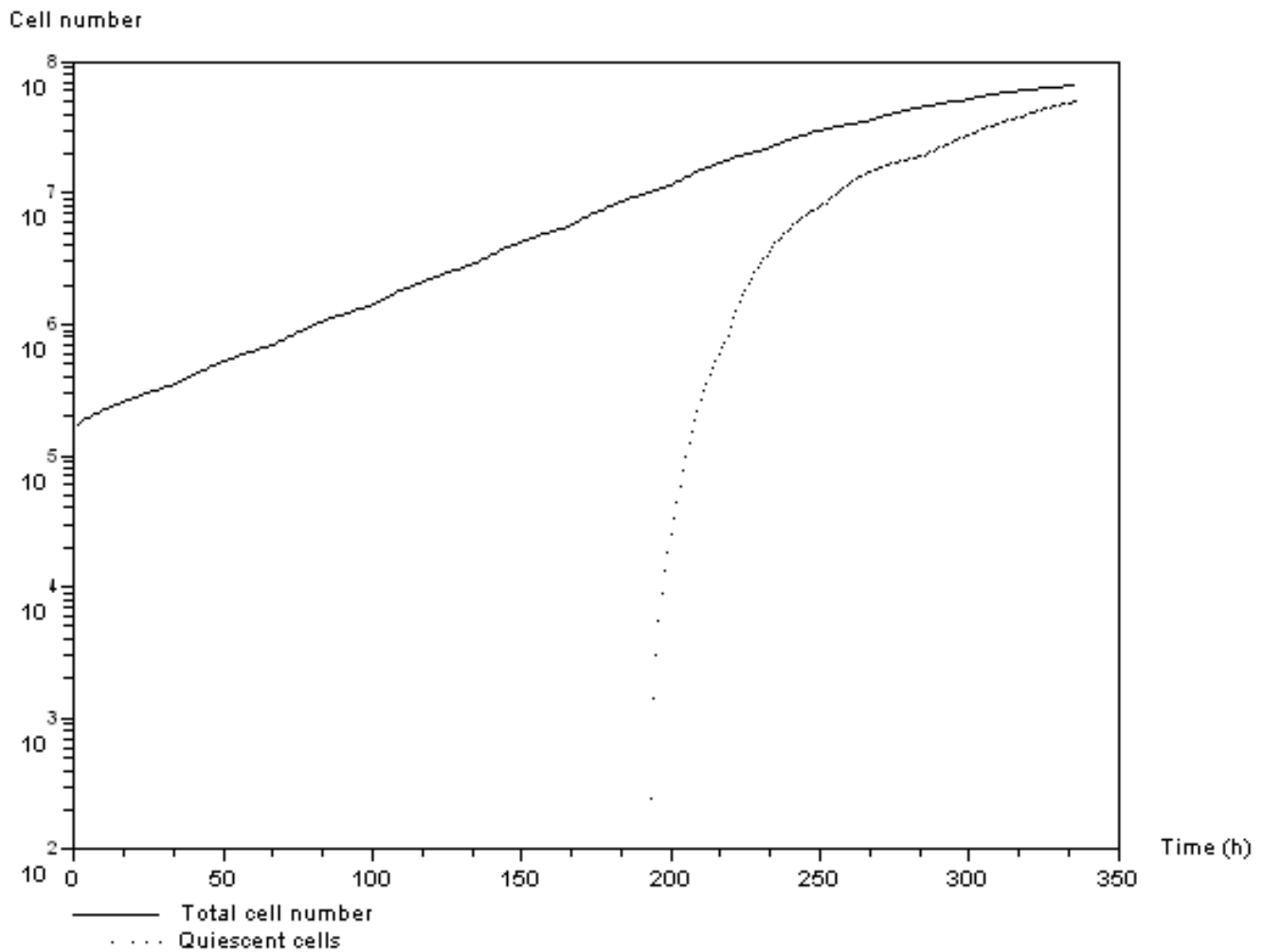


Figure 7
SMAD/RAS-dependent growth regulation. Evolution of the number of quiescent cells and total number of cells over time (log plot). An APC mutated cell population is regulated through SMAD/RAS activation due to hypoxia. Total number of cells (continuous line) and number of quiescent cells (dotted line).

SMAD/RAS-dependent growth regulation

Figure 7 shows the time courses of total cell number and quiescent cell number. In this figure, cells are APC mutated and the growth regulation is controlled by SMAD/RAS signaling, which has been activated by hypoxia. Before hypoxia, cell population growth is exponential and becomes more linear as the anti-growth signals start.

Figure 8 shows the evolution of the number of spatial units in the computational domain co-opted by the two regulation signals. The overpopulation and hypoxia signal

curves can be related to the evolution of the quiescent cells from Figure 6 and Figure 7 respectively. Figure 8 reveals the difference in evolution between the hypoxia and overpopulation signaling within the computational domain. The first oscillating growth phase depicted in Figure 6 is caused by the step-by-step evolution of the overpopulation signal activation. Hypoxia activation depicted in Figure 8 appears later and displays a sharp increase. While the overpopulation signal is local – it depends only on the local conditions – activation of the hypoxia signal is due to non-local effects. Oxygen absorbed by the cells at a particular position is not available for neighboring cells.

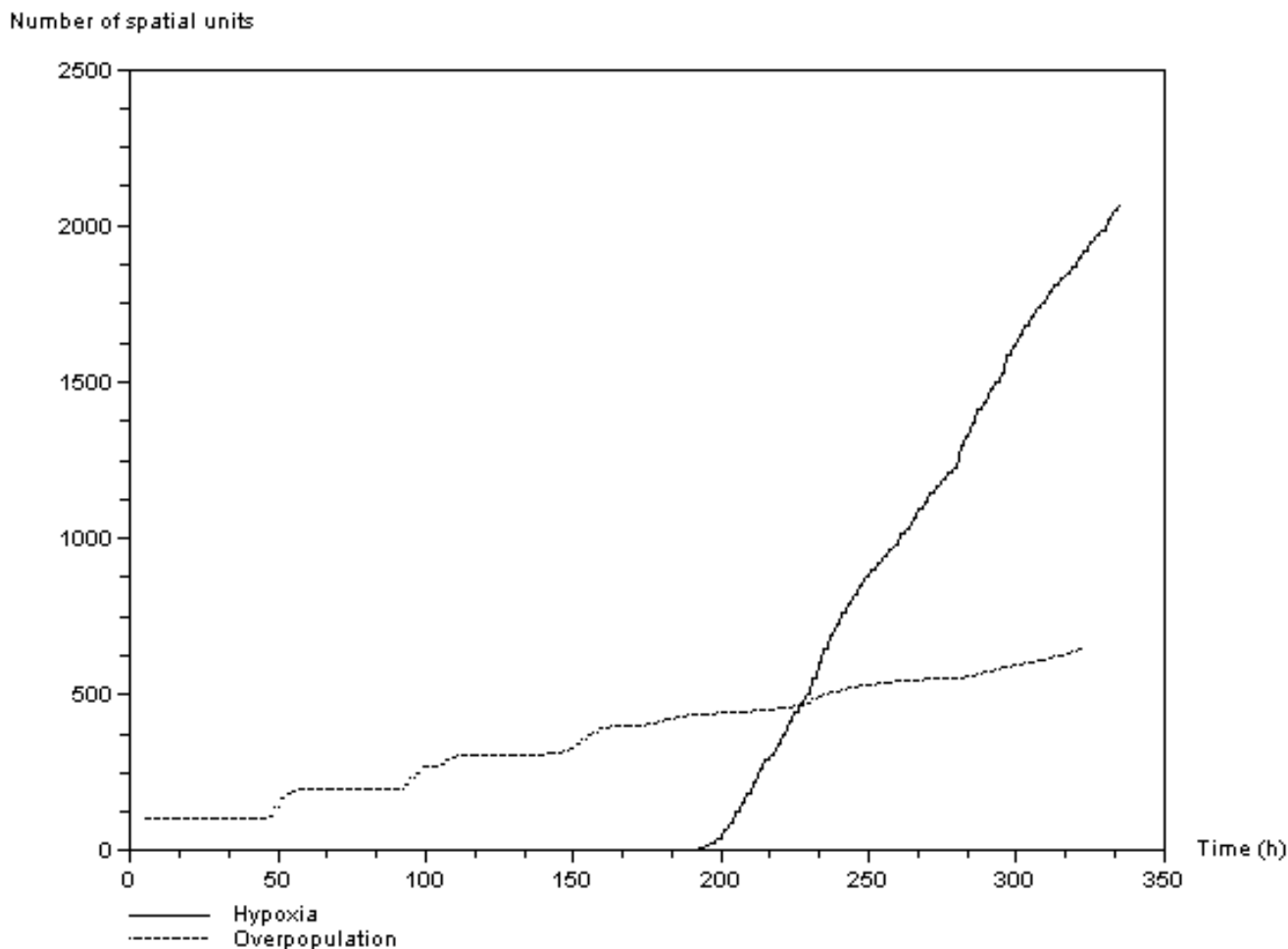


Figure 8

Anti-growth signals. Number of spatial units of the computation domain co-opted by the two regulation signals. The two curves show the activation of the hypoxia signal (continuous line) and the overpopulation signal (dashed line) over time. The vertical axis represents the number of elementary spatial units of the computational domain.

This results in regular signal propagation within the inner parts of the cell clusters as shown in the snapshots of Figure 9. Hypoxia starts from an outer area of the computational domain, i.e. areas more distant from the oxygen sources, and later occurs in the central cell cluster, where oxygen concentration is highest.

Influence of gene-dependent growth regulation on the response to irradiation protocols

Simulated irradiation protocols on APC and SMAD/RAS mutated tumor cells

Figure 10 shows the evolution of the number of mutated cells going through apoptosis due to the standard irradiation protocol. In our model the treatment damages a constant fraction of mitotic cells. APC and SMAD/RAS mutated cells are not sensitive to anti-growth signals; they

are in hypoxic and overpopulation conditions that lead mitotic cells to grow without regulation. Therefore the number of apoptotic cells is increased by the irradiation treatment. However, the number of apoptotic cells resulting from one treatment cycle is strictly equivalent to that induced by the previous therapeutic cycle. This is due to the difference between cell cycle duration (33 hours) and application of the treatment (24 hours).

Simulated irradiation protocols and APC-dependent tumor growth

When cells are sensitive to overpopulation (see growth curves Figure 6), population growth becomes linear after a first oscillating stage. Figure 11 shows the difference in efficacy between two irradiation protocols that are strictly equivalent in terms of the total dose delivered. The first is the standard protocol (dashed line), where the two doses

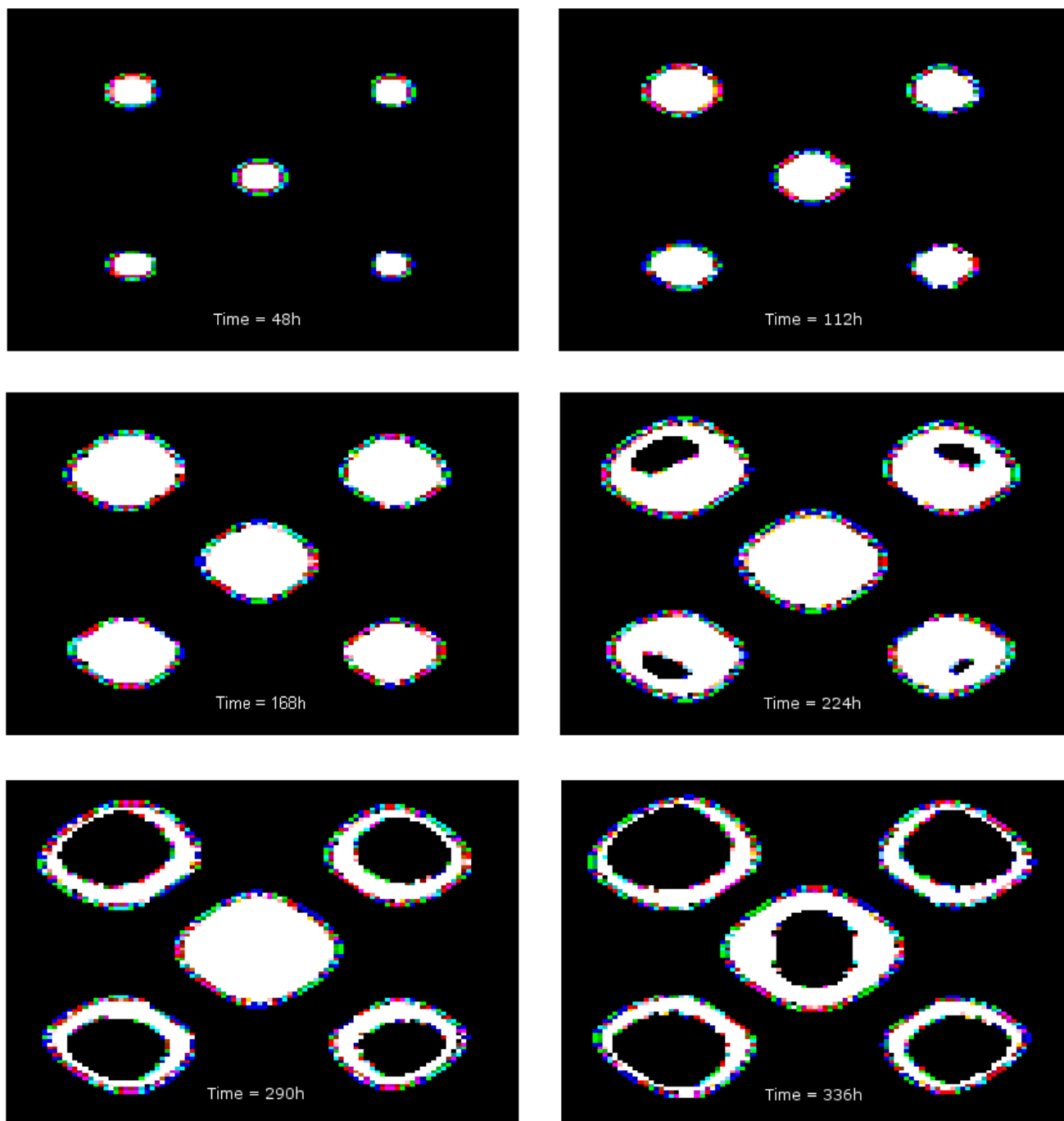


Figure 9
Evolution of the spatial distribution of mitotic cells. Temporal propagation of hypoxia signal within the tumor masses. Inner black areas are cells in quiescence due to *SMAD/RAS* activation through hypoxia. The spatial distribution of mitotic cells at: top-left 48 h, top-right 112 h, middle-left 168 h, middle-right 224 h, bottom-left 290 h, bottom-right 336 h.

are delivered with a 24 h interval. The second is a heuristic approach, in which we optimized delivery of the second dose by taking account of cell cycle regulation; the second treatment is given when the number of the mitotic cells

reaches a maximum. The first treatment application decreases the number of tumor cells. (Note that the dotted line in Figure 11 is hidden by the continuous line.) This also occurs in the second treatment of the heuristic proto-

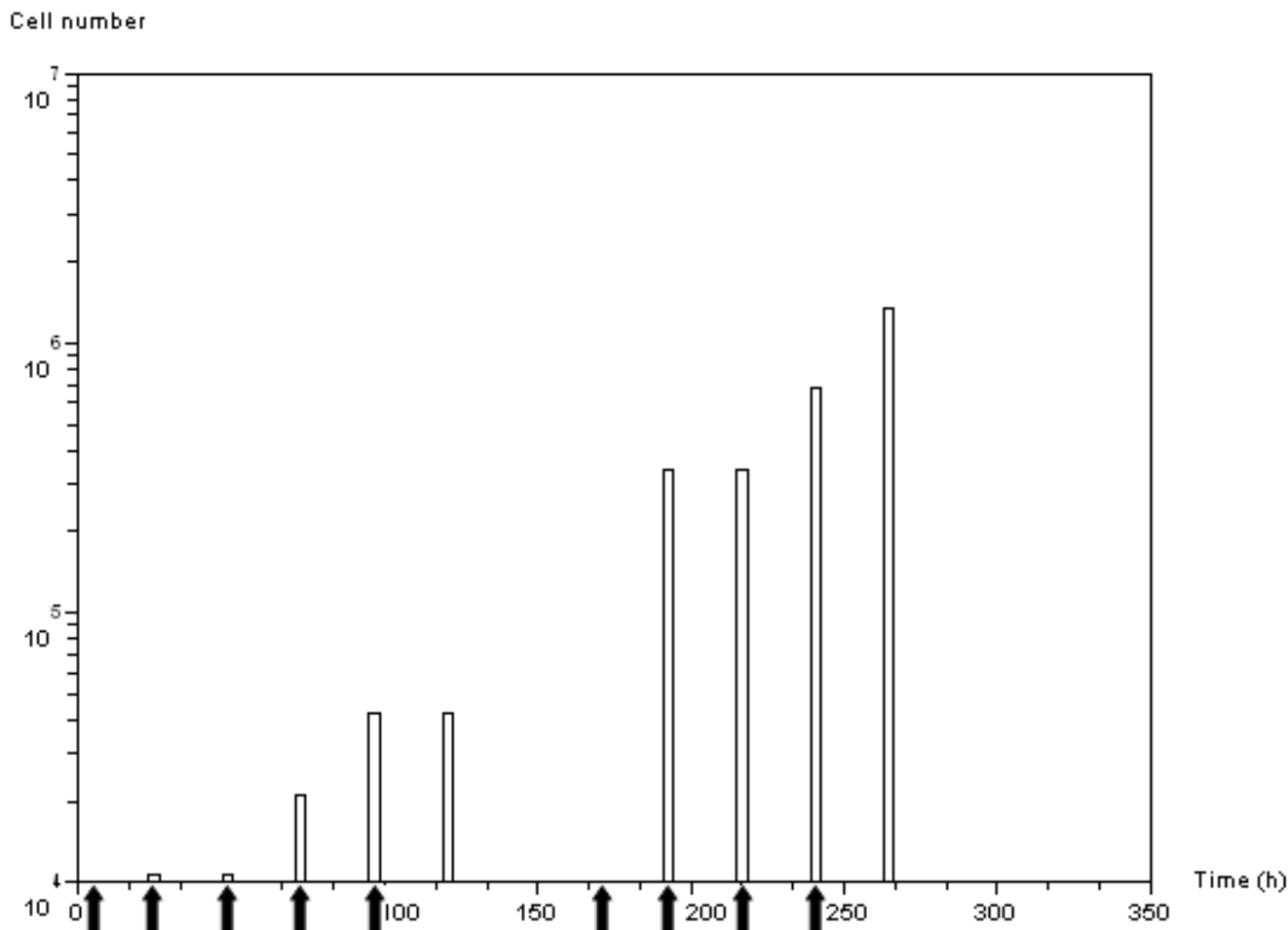


Figure 10
Apoptotic activity. Number of cells in the apoptotic phase over time when applying the standard radiotherapeutic protocol: 2 Gy daily. Vertical black arrows indicate treatment delivery times. Note that apoptotic activity appears at a fixed time after treatment delivery. This is the time needed for the G_2M DNA-injured cells to reach the restriction point of the cell cycle (21 hours according to the model parameters).

col. However, when the second treatment is delivered without taking growth regulation into account, i.e. standard scheduling, the efficacy is very poor (see Figure 11).

Simulated irradiation protocols on APC-mutated (SMAD/RAS-dependent) tumor growth regulation profiles

Figure 12 shows the evolution of the irradiated target cell population fraction, by which we mean the time course of the mitotic fraction without irradiation, before and after activation of the hypoxia signal. As soon as the hypoxia appears, the mitotic fraction collapses. Table 1 shows the difference in simulated efficacy between two equivalent protocols in terms of total dose. The first is the standard protocol, where the 2Gy treatments are given daily, 5 days a week for 2 weeks, with a total dose of 20Gy. The second is the heuristic treatment, in which all 10 doses of 2Gy are

given before the hypoxia signals appear. Part of the standard treatment is delivered while the tumors are becoming hypoxic (mitotic fraction falls), and this results in a decrease in efficacy. In contrast, all 10 doses in the heuristic treatment are delivered before hypoxia, which gives improved efficacy.

Sensitivity to model parameters and initial conditions

We study the potential influence of the choice of parameters values on the model's results. The most critical parameters to account for include:

- cell-specific radiosensitivity parameters (α_ϕ);

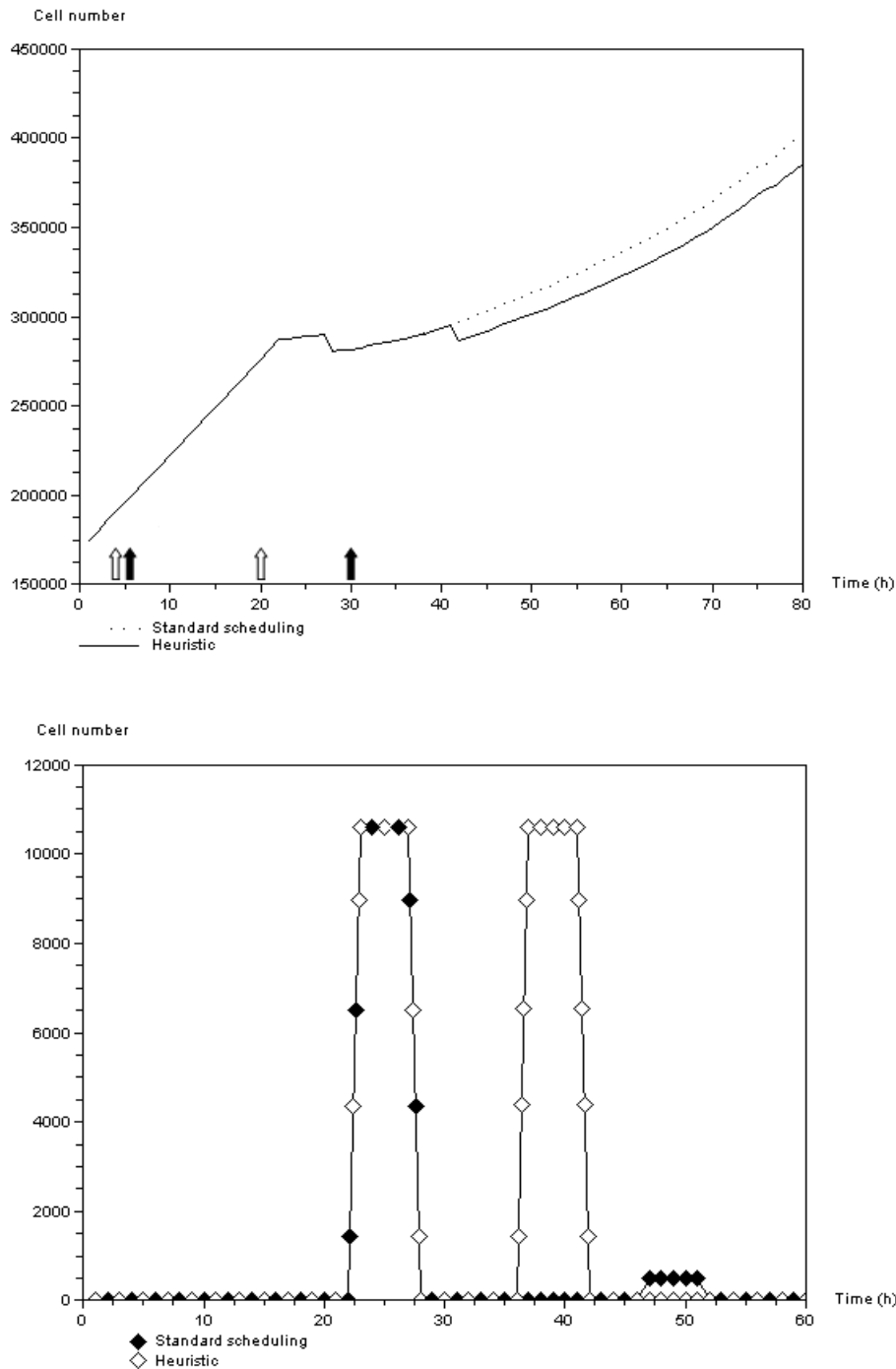


Figure 11

Comparison of two radiotherapeutic protocols. Top: Total cell number in response to standard therapeutic scheduling, i.e. 2 Gy applied twice within a 24 hour interval, and in response to a heuristic scheduling. Note that for the first 40 hours, the dotted line is superimposed on the continuous line since until the treatments diverge the populations are the same. Bottom: Evolution of the number of apoptotic cells due to irradiation protocols. The first treatment induces the same number of apoptotic cells. The effect of the second treatment in the standard protocol is negligible (black diamonds around time 50 h) in contrast to the heuristic approach (white diamonds pick at 40 h). Treatment delivery times are symbolized by vertical arrows: unfilled diamonds for the standard scheduling and solid diamonds for the heuristic approach.

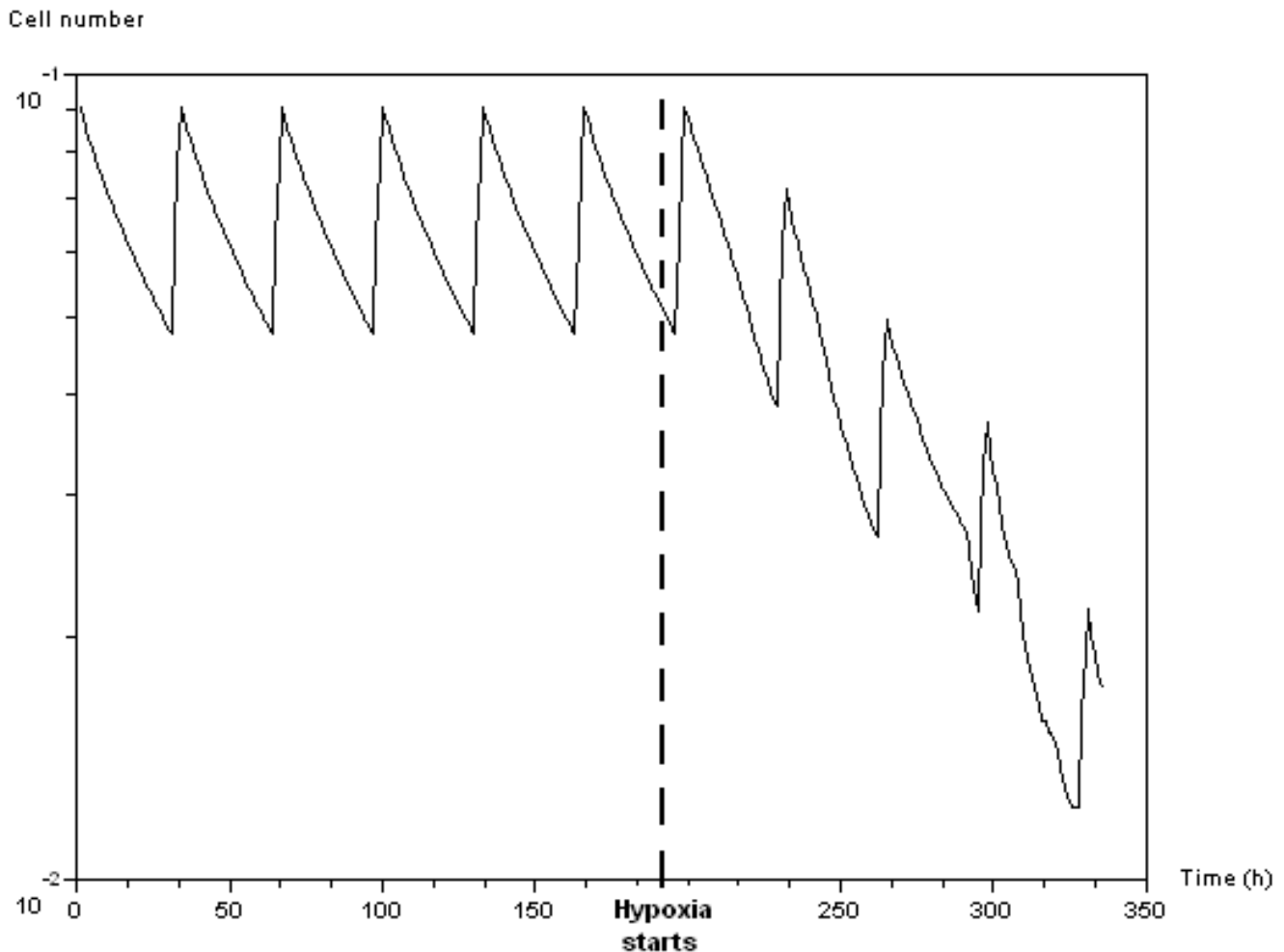


Figure 12
Evolution of simulated mitotic fraction of APC-mutated cells over time without irradiation. The vertical dashed line indicates the time when the hypoxia signal is activated.

- anti-growth signals, i.e. hypoxia and overpopulation, activation thresholds above which cells go into quiescence (Th_o and Th_t);
- initial conditions, i.e. initial number of cells and spatial configurations of oxygen sources.

Treatment protocol efficacy depends directly on cell-specific radiosensitivity parameters. Figure 13 compares the evolution of total cell number over time when the standard treatment protocol is applied. Model simulations show that the standard treatment is efficient when the parameters make cells in G_1 phase become radiosensitive. APC and SMAD/RAS activation, which leads cells to

become quiescent, is controlled by the two threshold parameters Th_t and Th_o . Increasing Th_t results in delay of the overpopulation signal, while increasing Th_o speeds hypoxia activation.

Decreasing the initial number of cells has the same effect as increasing Th_t , while decreasing the number or the initial strength of the oxygen sources has the same effect as increasing Th_o . The initial configuration of tumor cells and oxygen sources is important for spatial propagation of the hypoxia signal. Indeed, Figure 9 shows a particular hypoxia propagation in the tumor cell masses that is correlated with the locations of the oxygen sources. Since Th_t and Th_o are merely constants, it seems that we may change

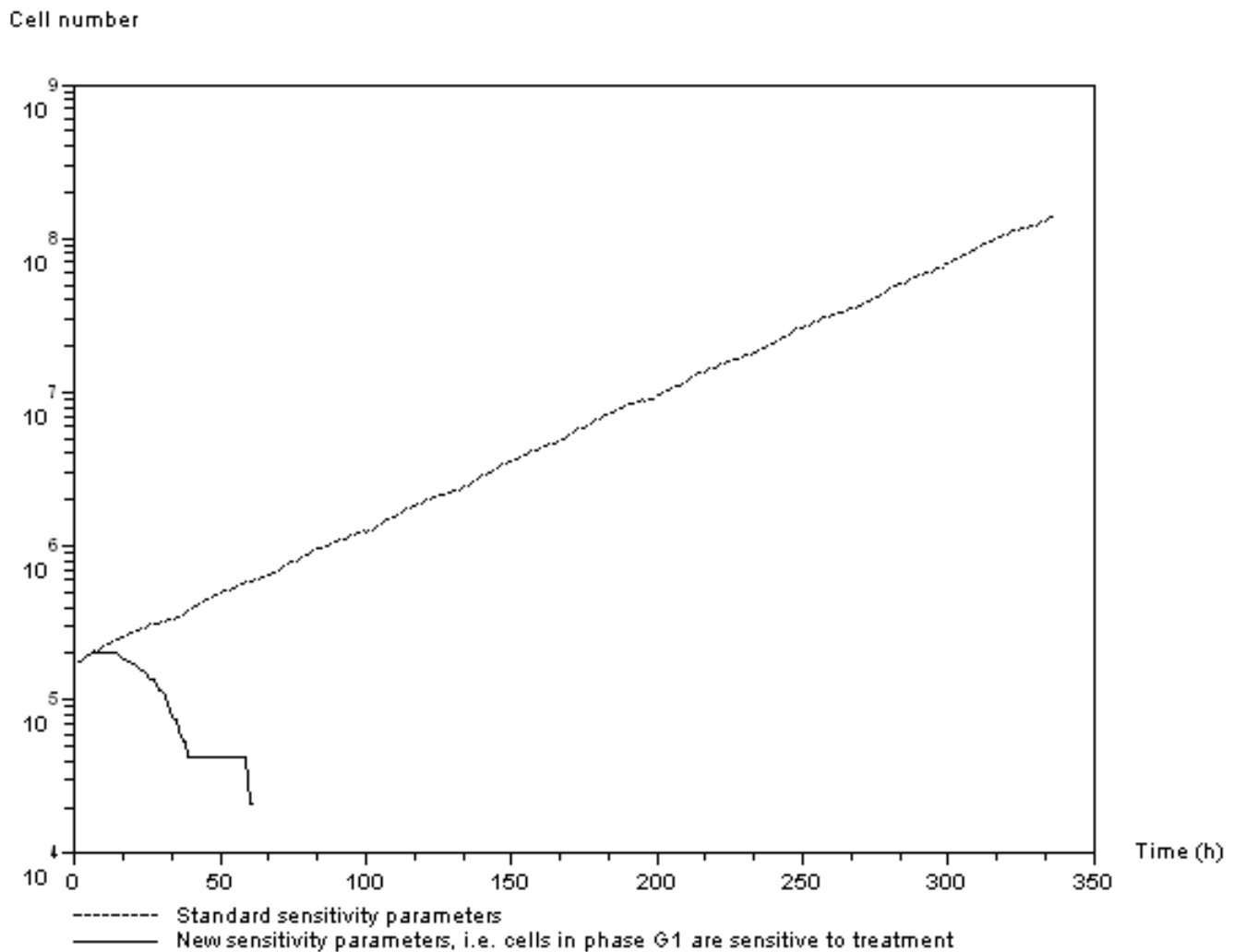


Figure 13

Effect of radiosensitivity parameters on treatment efficacy. Evolution of total cell number over time with the standard radiosensitivity parameters (continuous line), and with the suggested parameters. This shows that, with the new treatment, cells in G_1 phase are sensitive to the 2 Gy treatment dose.

the spatial configuration and size of the initial cell population and vary the oxygen sources and yet produce the same qualitative results.

Finally, Figure 14 shows the difference in evolution of the overpopulation signal over time if the initial distribution of cells in the clusters is uniform or random. The step by step evolution of overpopulation activation is softened but still exists when the cells are randomly distributed within the initial tumor masses.

Conclusion

We have presented a multiscale model of cancer growth and examined the qualitative response to radiotherapy. The mathematical framework includes a Boolean descrip-

tion of a genetic network relevant to colorectal oncogenesis, a discrete model of the cell cycle and a continuous macroscopic model of tumor growth and invasion. The basis of the model is that the sensitivity to irradiation depends on cell cycle phase and that DNA damage is proportional to the radiation dose. Anti-growth regulation signals such as hypoxia and overpopulation activate the *SMAD/RAS* and *APC* genes, respectively, and inhibit proliferation through cell cycle regulation.

Simulation results show the different features of the anti-growth signal activation and propagation within the tumor (see Figure 8). The overpopulation signal mediated by the *APC* gene initially induces oscillatory growth owing to a combination of proliferating and quiescent cells (see

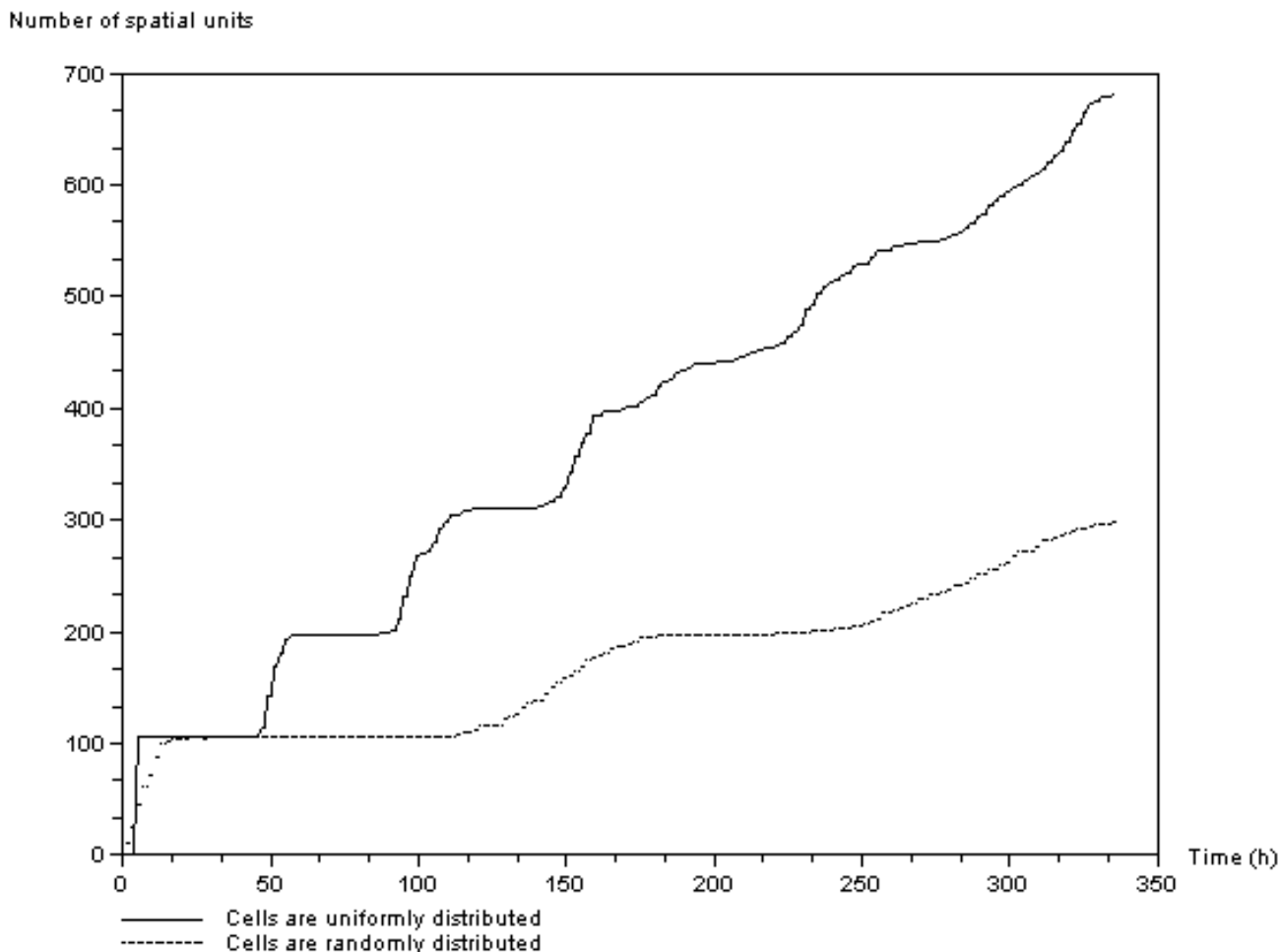


Figure 14

Effect of cell distribution within the initial cell clusters on overpopulation. The vertical axis is the number of elementary spatial units of the computational domain. Here we show the difference between evolution of the overpopulation signal over time when cells in the clusters are initially distributed uniformly or randomly. The evolution of overpopulation activation is softened but still exists when cells are randomly distributed within the initial tumor masses.

Figure 6). Because of its non-local effect, the hypoxia signal mediated by genes *SMAD/RAS* appears later but develops quickly within the tumor masses, and leads the mitotic fraction to collapse (see Figures 11 and 14). These features make the evolution of the number of quiescent cells and thus the efficacy of irradiation protocols depend on the type of anti-growth signals to which the tumors are exposed. Figure 11 and Table 1 show that efficacy could be improved, without increasing radiation doses, by planning schedules that take account of the features of tumor growth through cell cycle regulation.

The proposed framework emphasizes the significant role of gene-dependent cell-cycle regulation in the response of tumors to radiotherapy. Clinical studies have recognized *p53* status as a major predictive factor for the response of

rectal cancer to irradiation. Nevertheless, some results encourage investigation of other different factors [46]. In particular, it has been suggested that macroscopic factors such as hypoxia and tumor volumes are important [47]. The present modeling framework integrates these factors through cell cycle regulation and allows consideration of other factors at the genetic, cellular or tissue level.

Some modeling assumptions must be discussed. We chose a continuous approach that provides cell density rather than actual cell number. This assumes that the region of interest is large since we have restricted our analysis to late-stage tumor development. We have not considered cell shape, which has been shown to be important for the correct description of growth control processes [48]. Individual-based models of cell movement, e.g. the Potts

model [49,50] and the Langevin model [51], would improve our approach. We reduced the system to two dimensions. A three-dimensional tumor model could reveal new factors in the dynamics.

The aim of this study is to understand the qualitative effect of therapeutic protocols on colorectal cancer. Our analysis raises some interesting points about the influence of anti-growth regulation signals and genetic pathways on the efficacy of the standard protocol. Efforts have been made to improve the LQ model by taking into account multiple factors such as tumor volume and repopulation between treatment cycles [52]. However, we have produced a multiscale model that is more realistic and demonstrated its use in comparing efficacy of treatment protocols.

Authors' contributions

BR designed the mathematical multiscale model and simulated it to investigate the role of cell cycle regulation in response to irradiation treatment protocols. TC designed the macroscopic level. He implemented the advection-diffusion equations and contributed to linking the sub-models together. SS elaborated the genetic Boolean network model of colorectal oncogenesis and its implementation. He also supervised manuscript preparation and revision.

Acknowledgements

BR is funded by the ETOILE project: "Espace de Traitement Oncologique par Ions Légers dans le cadre Européen". Part of this work was carried out during the "Biocomplexity Workshop 7" held at Indiana University (Bloomington Campus) in May 9–12, 2005. The workshop was sponsored by the National Science Foundation (Grant MCB0513693) and the National Institute of General Medical Science/National Institutes of Health (Grant R13GM075730). BR is very grateful for the hospitality of the Indiana University School of Informatics and the Biocomplexity Institute during his visit May 8–14. The authors wish to acknowledge particularly the two referees for their useful comments; Professor Jean-Pierre Boissel and François Gueyffier for manuscript review; Professor Emmanuel Grenier, Dr Didier Bresch, and Nicolas Voirin for their valuable advice regarding model implementation; and Dr Ramon Grima and Edward Flach for critical comments.

References

- Brunton GF, Wheldon TE: **The Gompertz equation and the construction of tumor growth curves.** *Cell Tissue Kinet* 1980, **13**:455-460.
- Bassukas ID: **Comparative Gompertzian analysis of alterations of tumor growth patterns.** *Cancer Res* 1994, **54**:4385-4392.
- Skehan P, Friedman SJ: **Deceleratory growth by a rat glial tumor line in culture.** *Cancer Res* 1982, **42**:1636-40.
- Hart D, Shochat E, Agur Z: **The growth law of primary breast cancer as inferred from mammography screening trials data.** *Br J Cancer* 1998, **78**:382-387.
- Sachs RK, Hlatky LR, Hahnfeldt P: **Simple ODE models of tumor growth and anti-angiogenic or radiation treatment.** *Math Comput Model* 2001, **33**:1297-1305.
- Thames HD, Hendry JH: *Fractionation in Radiotherapy* London: Taylor and Francis; 1987.
- Kutcher GJ: **Quantitative plan evaluation: TCP/NTCP models.** *Front Radiat Ther Oncol* 1996, **29**:67-80.
- Pawlik TM, Keyomarsi K: **Role of cell cycle in mediating sensitivity to radiotherapy.** *Int J Radiat Oncol Biol Phys* 2004, **59**:928-942.
- Guichard M, Dertinger H, Malaise EP: **Radiosensitivity of four human tumor xenografts. Influence of hypoxia and cell-cell contact.** *Radiat Res* 1983, **95**:602-609.
- Ribba B, Marron K, Agur Z, Alarcon T, Maini PK: **A mathematical model of Doxorubicin treatment efficacy for non-Hodgkin's lymphoma: investigation of the current protocol through theoretical modelling results.** *Bull Math Biol* 2005, **67**:79-99.
- Ward JP, King JR: **Mathematical modelling of drug transport in tumour multicell spheroids and monolayer cultures.** *Math Biosci* 2003, **181**:177-207.
- Pettet GJ, Please CP, Tindall MJ, L MD: **The migration of cells in multicell tumor spheroids.** *Bull Math Biol* 2001, **63**:231-257.
- Alarcón T, Byrne HM, Maini PK: **Towards whole-organ modelling of tumour growth.** *Prog Biophys Mol Biol* 2004, **85**:451-472.
- Anderson AR, Chaplain MA: **Continuous and discrete mathematical models of tumor-induced angiogenesis.** *Bull Math Biol* 1998, **60**:857-899.
- Hahn WC, Weinberg RA: **Modelling the molecular circuitry of cancer.** *Nat Rev Cancer* 2002, **2**:331-341.
- Fearon ER, Vogelstein B: **A genetic model for colorectal tumorigenesis.** *Cell* 1990, **61**:759-767.
- Arends JW: **Molecular interactions in the Vogelstein model of colorectal carcinoma.** *J Pathol* 2000, **190**:412-416.
- Woo RA, McLure KG, Lees-Miller SP, Rancourt DE, Lee PW: **DNA-dependent protein kinase acts up-stream of p53 in response to DNA damage.** *Int J Radiat Oncol Biol Phys* 1998, **394**:700-704.
- Kastan MB, Onyekwere O, Sidransky D, Vogelstein B, Craig RW: **Participation of p53 protein in the cellular response to DNA damage.** *Cancer Res* 1991, **51**:6304-6311.
- Lu X, Lane DP: **Differential induction of transcriptionally active p53 following UV or ionizing radiation: defects in chromosome instability syndromes?** *Cell* 1993, **75**:765-778.
- Harris SL, Levine AJ: **The p53 pathway: positive and negative feedback loops.** *Oncogene* 2005, **24**:2899-2908.
- Yonish-Rouach E, Resnitzky D, Lotem J, Sachs L, Kimchi A, Oren M: **Wild-type p53 induces apoptosis of myeloid leukaemic cells that is inhibited by interleukin-6.** *Nature* 1991, **352**:345-347.
- Lewis TS, Shapiro PS, Ahn NG: **Signal transduction through MAP kinase cascades.** *Adv Cancer Res* 1998, **74**:49-139.
- Zhang H, Akman HO, Smith EL, Zhao J, Murphy-Ullrich JE, Batuman OA: **Cellular response to hypoxia involves signalling via Smad proteins.** *Blood* 2003, **101**:2253-2260.
- Akman HO, Zhang H, Siddiqui MA, Solomon W, Smith EL, Batuman OA: **Response to hypoxia involves transforming growth factor-beta2 and Smad proteins in human endothelial cells.** *Blood* 2001, **98**:3324-3331.
- Rubinfeld B, Souza B, Albert I, Muller O, Chamberlain SH, Masiarz FR, Munemitsu S, Polakis P: **Association of the APC gene product with beta-catenin.** *Science* 1993, **262**:1731-1734.
- Su LK, Vogelstein B, Kinzler KVV: **Association of the APC tumor suppressor protein with catenins.** *Science* 1993, **262**:1734-1737.
- Gottardi CJ, Wong E, Gumbiner BM: **E-cadherin suppresses cellular transformation by inhibiting beta-catenin signaling in an adhesion-independent manner.** *J Cell Biol* 2001, **153**:1049-1060.
- Brocardo MG, Bianchini M, Radrizzani M, Reyes GB, Dugour AV, Taminelli GL, Gonzalez Solveyra C, Santa-Coloma TA: **APC senses cell-cell contacts and moves to the nucleus upon their disruption.** *Biochem Biophys Res Commun* 2001, **284**:982-6.
- Hulsken J, Behrens J, Birchmeier W: **Tumor-suppressor gene products in cell contacts: the cadherin-APC-armadillo connection.** *Curr Opin Cell Biol* 1994, **6**:711-716.
- Boman BM, Walters R, Fields JZ, Kovatich AJ, Zhang T, Isenberg GA, Goldstein SD, Palazzo JP: **Colonic crypt changes during adenoma development in familial adenomatous polyposis: immunohistochemical evidence for expansion of the crypt base cell population.** *Am J Pathol* 2004, **165**:1489-1498.
- Kauffman SA: **Metabolic stability and epigenesis in randomly constructed genetic nets.** *J Theor Biol* 1969, **22**:437-467.
- Thomas R: **Boolean formalization of genetic control circuits.** *J Theor Biol* 1973, **425**:563-585.
- Thomas R, D'Ari R: *Biological Feedback* Ann Arbor, Boston: CRC Press, Boca Rato; 1990.
- Potten CS, Kellett M, Roberts SA, Rew DA, Wilson GD: **Measurement of in vivo proliferation in human colorectal mucosa using bromodeoxyuridine.** *Gut* 1992, **33**:71-78.

36. Blagosklonny MV, Pardee AB: **The restriction point of the cell cycle.** *Cell Cycle* 2000, **1**:103-110.
37. Kufe DW, Pollock RE, Weichselbaum RR, Bast RC, Gansler TS, Holland JF: *Cancer Medicine* 6th edition. Hamilton (Canada): BC Decker Inc; 2003.
38. Ambrosi D, Preziosi L: **On the closure of mass balance models for tumor growth.** *Math Models Method Appl Sci* 2002, **12**:737-754.
39. Greenspan HP: **Models for the Growth of a Solid Tumor by diffusion.** *Stud Appl Math* 1972, **LI**,4:317-340.
40. Greenspan HP: **On the growth and stability of cell cultures and solid tumors.** *J Theor Biol* 1976, **56**:229-242.
41. Bischof M, Huber P, Stoffregen C, Wannemacher M, Weber KJ: **Radiosensitization by pemetrexed of human colon carcinoma cells in different cell cycle phases.** *Int J Radiat Oncol Biol Phys* 2003, **57**:289-292.
42. Darrouti F, Vyas RC, Vermeulen S, T NA: **G2 radiosensitivity of cells derived from cancerprone individuals.** *Mutat Res* 1995, **328**:83-90.
43. Latz D, Schulze T, Manegold C, Schraube P, Flentje M, J WK: **Combined effects of ionizing radiation and 4-hydroperoxyfosfamide in vitro.** *Radiother Oncol* 1998, **46**:279-283.
44. Rew DA, Wilson GD, Taylor I, Weaver PC: **Proliferation characteristics of human colorectal carcinomas measured in vivo.** *Br J Surg* 1991, **78**:60-66.
45. Kinzler KVV, Vogelstein B: **Lessons from hereditary colorectal cancer.** *Cell* 1996, **87**:159-170.
46. Lopez-Crapez E, Bibeau F, Thezenas S, Ychou M, Simony-Lafontaine J, Thirion A, Azria D, Grenier J, Senesse P: **p53 status and response to radiotherapy in rectal cancer: a prospective multilevel analysis.** *Br J Cancer* 2005, **92**:2114-2121.
47. Dubben HH, Thames HD, Beck-Bornholdt HP: **Tumor volume: a basic and specific response predictor in radiotherapy.** *Radiother Oncol* 1998, **47**:167-174.
48. Folkman J, Moscona A: **Role of cell shape in growth control.** *Nature* 1978, **273**:345-349.
49. Galle J, Loeffler M, Drasdo D: **Modeling the effect of deregulated proliferation and apoptosis on the growth dynamics of epithelial cell populations in vitro.** *Biophys J* 2005, **88**:62-75.
50. Graner F, Glazier JA: **Simulation of biological cell sorting using a two-dimensional extended Potts model.** *Phys Rev Lett* 1992, **69**:2013-2016.
51. Newman TJ, Grima R: **Many-body theory of chemotactic cell-cell interactions.** *Phys Rev E Stat Nonlin Soft Matter Phys* 2004, **70**:051916.
52. M WL, Cohen JE, Wu JT: **Dynamic optimization of a linear-quadratic model with incomplete repair and volume-dependent sensitivity and repopulation.** *Int J Radiat Oncol Biol Phys* 2000, **47**:1073-1083.
53. Kanehisa M: **A database for post-genome analysis.** *Trends Genet* 1997, **13**:375-376.
54. Kanehisa M, Goto S: **KEGG: Kyoto Encyclopedia of Genes and Genomes.** *Nucleic Acids Res* 2000, **28**:27-30.

Publish with **BioMed Central** and every scientist can read your work free of charge

"BioMed Central will be the most significant development for disseminating the results of biomedical research in our lifetime."

Sir Paul Nurse, Cancer Research UK

Your research papers will be:

- available free of charge to the entire biomedical community
- peer reviewed and published immediately upon acceptance
- cited in PubMed and archived on PubMed Central
- yours — you keep the copyright

Submit your manuscript here:
http://www.biomedcentral.com/info/publishing_adv.asp

